Towards the understanding of mechanical properties of super- and ultrahard nanocomposites

Stan Veprek[a)]
Institute for Chemistry of Inorganic Materials, Technical University Munich, Lichtenbergstr. 4, D-85747 Garching b. Munich, Germany

Ali S. Argon
Department of Mechanical Engineering, Massachusetts Institute of Technology, 77 Massachusetts Avenue, Cambridge, Massachusetts 02139

(Received 6 June 2001; accepted 21 January 2002)

This article presents an attempt to explain in a simple way, understandable to a broad spectrum of readers, the unusual combination of the mechanical properties of the recently developed new class of superhard nanocomposites, such as high hardness which significantly exceeds that of the rule of mixtures, enhancement of the elastic modulus as measured by the indentation technique, very high elastic recovery which is observed upon the indentation and the absence of crack formation even under elastic deformation corresponding to a strain of more than 10%. Future experimental work is suggested which should bring further progress towards the understanding of these materials. [DOI: 10.1116/1.1459722]

I. INTRODUCTION

Super- and ultrahard materials are defined as those with Vickers hardness H_V of 40–60 and $\geqslant$70 GPa, respectively.[1] The only super- and ultrahard materials which are available as single crystals are cubic boron nitride (c-BN, $H_V \approx 48$ GPa) and diamond ($H_V \approx 70-90$ GPa) due to the high strength of their covalent interatomic bond, small bond distance, and high coordination number.[2] Because the presence of inherent flaws, such as dislocations with some mobility and microcracks, limits the practically achievable strength and hardness of materials by orders of magnitude as compared to the ideal behavior,[3–5] it is possible to achieve superhardness in a variety of synthetic made materials by an appropriate design of their nanostructure which will hinder the movement and multiplication of dislocations and crack growth and in such a way enhance the practically achievable strength of that material by a factor of 3–4, still far below the ideal one. There are two classes of nanostructured superhard materials:[6]

(1) epitaxial and polycrystalline heterostructures and
(2) nanocomposites.

The strengthening of materials in heterostructures of a few nanometer thickness, consisting of multilayers made of alternating materials with different elastic moduli, was suggested by Koehler[7] and, later on, experimentally confirmed by a number of workers (for recent reviews see Refs. 6, 8, and 9). If such heterostructures are made of hard transition metal nitrides, their hardness can exceed 40 GPa. The originally suggested[7] mechanism of strengthening in the heterostructures was confirmed[8,9] and extended[10,11] by several researchers.

A variety of superhard nanocomposites made of nitrides, borides, and carbides was prepared by plasma induced techniques, such as plasma chemical vapor deposition (CVD) vacuum arc evaporation and reactive sputtering (physical vapor deposition, PVD).[6] In the appropriately synthesized binary systems the hardness of the nanocomposite exceeds significantly that given by the rule of mixtures in bulk. For example, the hardness of nc-M_nN/a-Si_3N_4 (M=Ti,W,V,…) nanocomposites with the optimum content of Si_3N_4 close to the percolation threshold reaches 50 GPa,[12–16] although that of the individual nitrides does not exceed 21 GPa in bulk.[17–20] Another example of such superhard nanocomposites is the Ti–B–N system (for the original articles see Ref. 6). In contrast, a binary solid solution, such as $TiN_{1-x}C_x$, shows a monotonous increase of the hardness with x increasing from 0 ($H_V \approx 22$ GPa for TiN) to 1 ($H_V \approx 40$ GPa for TiC),[16] thus following the rule of mixtures.

More recently, Musil *et al.* have demonstrated that superhardness can be achieved also in coatings consisting of a hard transition metal nitride with a few at.% of soft metal which does not form thermodynamically stable nitrides, such as nc-M_nN/M' (M=Ti, Cr, Zr, M′=Cu, Ni).[21–25] However, coatings, such as ZrN/Ni and CrN/Ni, prepared by these researchers have shown a low thermal stability because the superhardness results from the high compressive stress which decreases upon annealing at temperatures of $\geqslant$450 °C and the hardness decreases to that of the bulk materials.[26] No contribution to the enhanced hardness of the as deposited films due to the nanostructure could be found in the nc-M_nN/M' coatings so far.

The enhancement of the apparent hardness and elastic modulus in thin films due to a high biaxial compressive stress is commonly observed in PVD films deposited at a low pressure where the compressive stress can achieve values of 6–8 GPa or more (see, e.g., Refs. 6, 27, and 28 and references therein). For example, Herr and Broszeit[29] reported a

a)Electronic mail: veprek@ch.tum.de

hardness of 72 GPa for HfB_2 coatings sputter deposited at a low pressure of 5×10^{-3} mbar which introduced a high compressive biaxial residual stress of about 7 GPa. Upon annealing at 650 °C the stress and the hardness decreased to 2 and 17 GPa, respectively. Musil *et al.*[30] reported hardness of 100 GPa for (TiAlV)N films deposited by sputtering at low pressure and having also a high biaxial compressive stress. Unfortunately, the authors did not do any annealing experiments in order to verify what the real, ''intrinsic'' hardness of their films was. Nevertheless, the hardness of TiN coatings of about 80 GPa reported in the same article and of 70 GPa reported by the same author in a later publication[31] clearly shows that these measured values were falsified by the high compressive stress[32] which, in the plasma PVD films, is induced by energetic ion bombardment as already shown many years ago by Hoffman and Gaertner.[33] More recently, it has been shown that the apparent enhancement of the hardness of an aluminum alloy measured by the load-depth sensing indentation technique is an artifact since no change of Vickers hardness and elastic modulus was found when the size of the projected area of the remaining plastic deformation was measured optically.[27] This effect was explained in terms of pileup.[28] Because of such possibilities of incorrect hardness measurement and the low thermal stability of the nc-M_nN/M' coatings we shall concentrate in this article on those systems, where such enhancement of the apparent hardness due to compressive stress can be excluded and the superhardness is unambiguously related to the nanostructure.

The abovementioned plasma CVD deposited superhard nanocomposite films have a small compressive stress of $\leqslant 1$ GPa.[34] A high compressive stress of 3–5 GPa can also be induced in plasma CVD films if the substrate bias during the deposition amounts to -300 to -500 V.[35,36] Moreover, these nanocomposites possess a high thermal stability because the hardness did not change after annealing up to the recrystallization temperature of the nanocomposites of 900–1100 °C.[34,37,38]

The generic concept for the design of novel, superhard nanocomposites that are stable up to high temperatures of 1000 °C, which is very important for their industrial applications, is based on thermodynamically driven segregation in binary (and ternary) systems which display immiscibility and undergo spinodal decomposition even at such temperatures.[6,13–16,37–39] The condition for spinodal decomposition[40,41] in a binary system $A_{1-x}B_x$ to occur is a negative second derivative of the free energy of formation of the mixed phase $A_{1-x}B_x$ with an infinitesimal change of the composition $A_{1-x\pm\delta}B_{x\pm\delta}$, Eq. (1):

$$\frac{\partial^2 \Delta G^0(A_{1-x}B_x)}{\partial x^2} < 0. \tag{1}$$

This means that any small, local fluctuation of the composition of the mixed phase decreases the free energy of the system thus leading to a spontaneous segregation without any need for nucleation of either phase. The secondary phase forms a continuous network with a characteristic spatial separation (''crystallite size'') of which the dimension is given by the balance between the decrease of the free energy of the mixture upon the phase separation and the strain energy of the interface.[40,41] As a result, a stable nanocomposite forms.

Such a nanostructure remains stable against coarsening (Ostwald ripening) as long as condition (1) holds because any local fluctuation of the composition towards mixing increases the free energy of the system. Therefore, any system which meets this condition at high temperatures will not undergo Ostwald ripening (coarsening) thus retaining its nanostructure as well as the mechanical properties which are derived from that nanostructure.

II. MECHANICAL PROPERTIES OF SUPERHARD NANOCOMPOSITES

The most important and to some extent surprising properties of these materials are the strong enhancement of the elastic modulus up to the values of diamond, high hardness, and elastic recovery combined with a high resistance against crack formation. Because these materials were so far prepared as thin coatings by gas phase deposition processes, the mechanical properties were measured by indentation techniques. In the majority of published articles the load-depth sensing technique using modern automated instruments was used. Besides the abovementioned apparent enhancement of the hardness due to compressive stress, this technique may be subject to a number of errors unless the necessary care is taken to prevent them (see Refs. 6, 27, 28, 42–46 and references therein). In the case of the superhard nanocomposite coatings to be discussed here the reported values of the hardness measured by means of the indentation technique were confirmed by comparison with Vickers hardness obtained from the evaluation of the size of the remaining plastic deformation by means of scanning electron microscope (SEM).[6,38,47–49] Because the compressive stress in these coatings is also low and the applied load used for the measurements sufficiently high, the values of the plastic hardness reported in these articles are correct.

As the next step we shall check if the very high elastic recovery of the coatings measured upon the indentation meets the criteria of the Hertzian analysis of a reversible elastic deformation of an ideally elastic sphere in contact with a flat semi-infinitive elastic body.[50] Figure 1 shows as example typical indentation curves for a single phase nanocrystalline diamond[51] and ultrahard nc-TiN/a-Si_3N_4/a- and nc-$TiSi_2$ nanocomposite coatings.[47–49] The loading curve (lower curve) starts at zero and with increasing load the indentation depth increases up to the maximum, followed by the unloading curve (upper curve) which for $L\rightarrow 0$ approaches a finite value of the remaining indentation depth. The plastic hardness is calculated from the so-called ''corrected indentation depth,'' h_{corr}, which is obtained by the extrapolation of the linear part of the unloading curve to $L=0$. This is justified only in the case if, during the linear part of the unloading curve, the contact area between the indenter and the material under study remains constant (see Refs. 6, 42–45 and references therein). The ''effective'' elastic

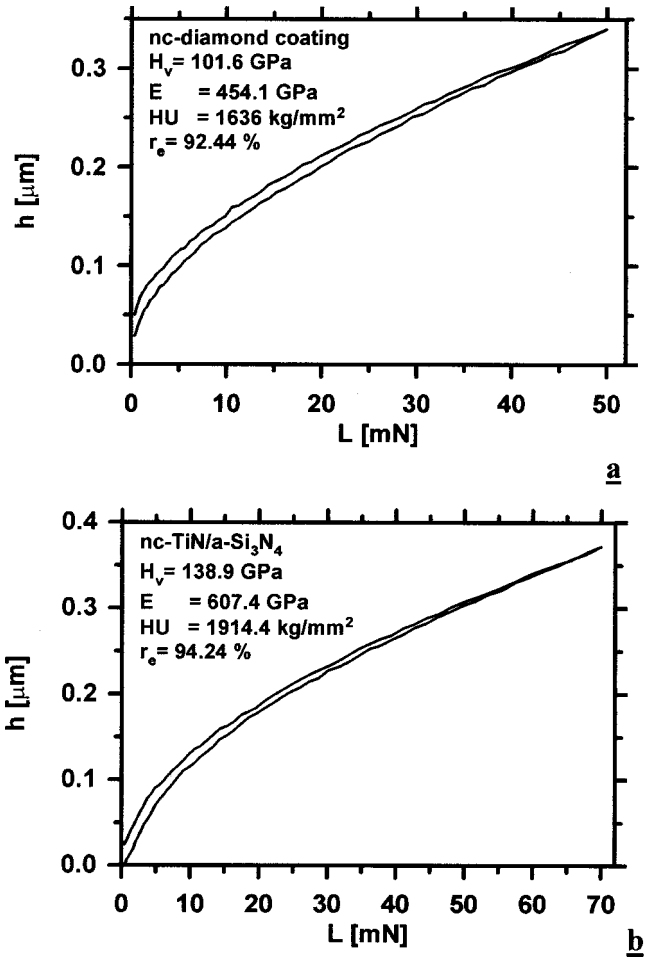

FIG. 1. Examples of indentation curves for single phase nanocrystalline diamond (see Ref. 51) and 3.5 μm thin ultrahard nanocomposites nc-TiN/a-Si_3N_4/a- and nc-$TiSi_2$ (see Ref. 38). The insets means the Vickers hardness H_V, elastic ("indentation") modulus E, universal hardness HU ("hardness under load"), and elastic recovery r_e.

modulus is calculated from the slope of this part of the unloading curve dL/dh and corrected for the elastic deformation of the indenter to obtain the elastic modulus of the material.[42–45]

For the purpose of further discussion it is important to note that the elastic modulus is evaluated from the elastic response of the indented material under a high load close to $L_{\max}$. The area between the loading curve and the axis of the indentation depth (here the vertical one) is the total energy of the deformation, the area between the unloading curve and that axis is the energy of the elastic deformation and the area between the loading and unloading curve is the dissipated energy of the plastic deformation which is a measure of the hardness. The smaller the ratio of the dissipated energy of plastic deformation to that of the total energy of deformation, the higher the plastic hardness.[52–54] The higher the ratio of the energy of elastic to plastic deformation, the higher is the elastic recovery.

Although the shape of the loading and unloading curves in Fig. 1 clearly supports the view of predominantly elastic nature of the deformation, and also the high value of the

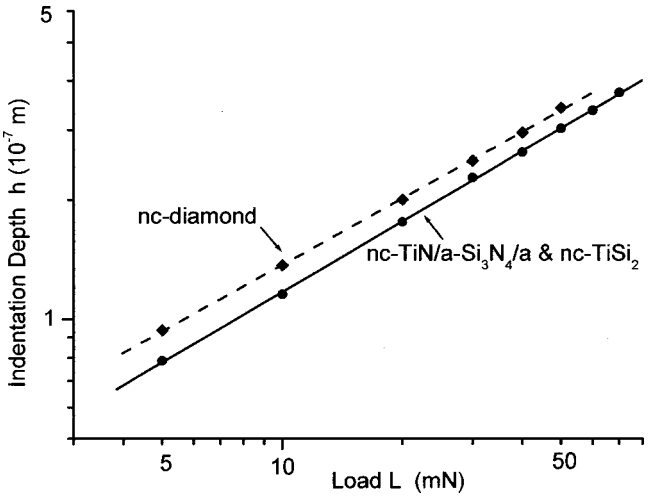

FIG. 2. "Hertzian" plot of the indentation depth $h(L)$ vs applied load L.

"universal hardness" HU (the hardness under load, see inserts in Figs. 1(a) and 1(b) underlines the high strength of the material, it is important to check if the nature of the indentation meets the criterion of elastic indentation response according to classical Hertzian indentation solution. In first approximation this can be assessed by means of the Hertzian elastic response under spherical indenter of radius R and contact circle radius a (for details see Ref. 50). For simplicity we assume the same elastic moduli of the indenter and the coating because of the close agreement of these values as found in Fig. 1 and many other measurements on such coatings. The analysis of the Hertzian indentation of elastic spherical indenter of radius R into an elastic, semi-infinitive material gives a dependence of the indentation depth $h(L)$ on the applied load L:

$$\ln h(L) = \frac{1}{3}\left[-\ln\left(\frac{E^2 \cdot R}{1.861}\right)\right] + \frac{2}{3}\ln L. \tag{2}$$

Digitizing the $h(L)$ vs L behavior in the nanostructured diamond ($E = 454$ GPa) and the nanostructured TiN/Si_3N_4/$TiSi_2$ ($E = 607$ GPa) coatings (Fig. 1) gives the dependence shown in Fig. 2. It shows a very good log–log straight line behavior with slopes 0.585 and 0.6 for the nanostructured diamond and TiN/Si_3N_4/$TiSi_2$, respectively. The relatively small difference from the true Hertzian slope for ideally elastic materials of $2/3 = 0.667$ can be attributed to the fact that the indentations are not purely elastic and that the indenter geometry of the Vickers diamond is not exactly spherical as well as the significant distortion of the indenter.

Moreover, taking the plot of Fig. 2 and the elastic moduli of the materials of the coatings, the radius of the tip of the indentor can be calculated from Eq. (3):[50]

$$h = 1.23\left(\frac{L^2}{E^2 \cdot R}\right)^{1/3}. \tag{3}$$

The resultant values of $R = 0.448$ and $0.385\,\mu$m for nc-diamond and TiN/Si_3N_4/$TiSi_2$ coatings are in a reason-

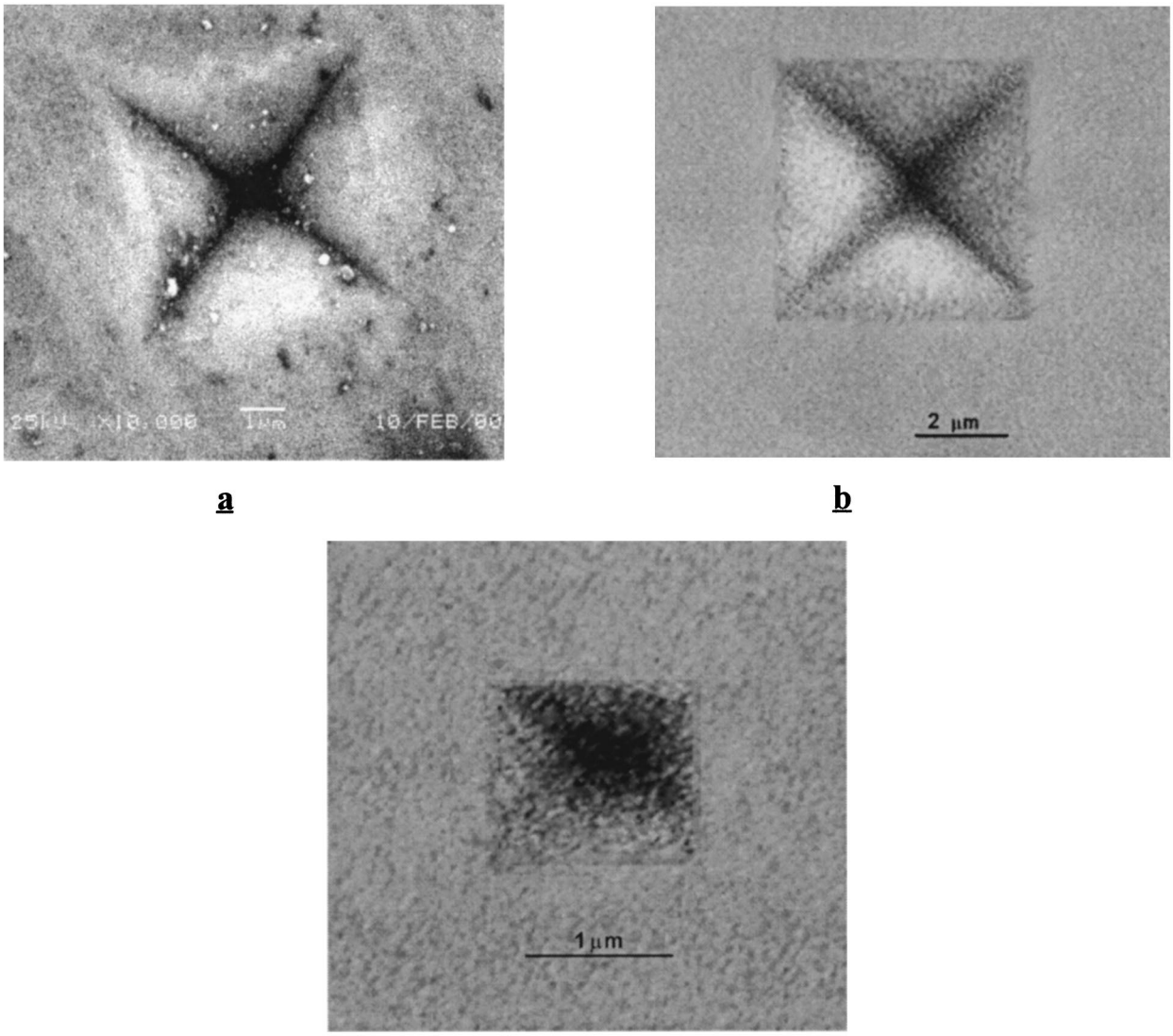

FIG. 3. Examples of the appearance of the remaining indentation into: (a) 6.1-μm-thick ultrahard coating ($H_{0.005} \approx 100$ GPa) after applied load of 1000 mN; (b) 10.7-μm-thick superhard coating ($H_{0.01} \approx 40$ GPa) with a load of 1000 mN; (c) 3.5-μm-thick ultrahard coating from Fig. 1(b) after applied load of 100 mN (from Refs. 6 and 47).

ably good agreement with each other and with the radius of the Vickers diamond indenter of $\leqslant 0.5$ μm.[44]

This analysis shows clearly that the major portion of the h vs L response as measured by the indentation into the super- and ultrahard nanocomposite coatings is a simple Hertzian elastic indentation. This conclusion is also supported by Fig. 3 which shows typical examples of the SEM micrographs of the remaining plastic deformation. The absence of cracks even after the indentation into the 6.1 μm thin coatings with 1 N load [Fig. 3(a)], where the soft steel substrate is severely plastically deformed (depth of the plastic indentation in the steel of about 2 μm), lends an additional, strong support to this conclusion. Furthermore, the high values of the elastic moduli and of the universal hardness (hardness under the maximum applied load) underline the fact that these materials are indeed very strong, and that the observed extraordinary high ''plastic hardness'' is not due to any ''rubber-like'' elastic response. (See *Note Added in Proof* and Refs. 134 and 135.)

A. Origin of apparent enhancement of elastic modulus

The well known, approximate linear dependence of the hardness of crystals on the value of shear modulus G is explained by crystal plasticity (multiplication and movement of dislocations)[55,56] because the dislocation energy is proportional to G.[2–5] In the original publications, Veprek *et al.* reported a proportionality between the values of plastic hardness and elastic modulus measured by the indentation technique for several superhard nanocomposite systems[13–16]

and similar proportionality was found also for other systems by other workers. The proportionality between the measured values of Young's modulus and the hardness was reported also for a number of metallic glasses,[57–59] amorphous hydrogenated carbon (a-C:H), and silicon (a-Si:H)[60] with the proportionality factor varying between about 15 and 17 for the metallic glasses and 9 and 11 for a-C:H and a-Si:H, respectively. For the values of hardness extrapolated to zero the values of Young's modulus approached zero as well. The explanation of this relationship was based on the relation between yield stress and Vickers hardness

$$\sigma_{\text{Yield}} \approx H_V/3 \tag{4}$$

which was found by Tabor for metals[54] with little strain hardening and theoretically justified by Hill in terms of slip line field analysis.[61] Substituting the Hooke's law into that relationship, one obtains for the critical yield strain ϵ_{Yield}:

$$\epsilon_{\text{Yield}} \approx \frac{H_V}{3 \cdot E_Y}. \tag{5}$$

Therefore it has been suggested that the proportionality between the measured Young's modulus and hardness means, for a given type of material, a constant yield strain within the whole range of measured values and that the different values of the proportionality factor for different classes of materials reflect the differences in the values of the critical yield strain ϵ_{Yield}.[59,60]

However, the correlation $\sigma_{\text{Yield}} \approx H_V/3$ is not universally valid for all materials, such as brittle ceramics, glasses, and others which display a high ratio of the yield stress to Young's modulus $\sigma_{\text{Yield}}/E_Y$. The original derivation of relation (4) by Tabor was based on the assumption of the indentation of a hard, undeformable flat punch into an ideally plastic metal under a negligible friction (see Ref. 54 p. 34 ff.). This assumption is also included in the theoretical development of Hill.[61] The experimental verification was done on highly worked (in order to avoid any further work hardening upon the indentation experiment) metals, such as tellurium–lead alloy, aluminum, copper, and mild steel.

Later on Marsh has, however, shown that the Tabor's approximation (4) applies only for materials with a relatively low value of the ratio $\sigma_{\text{Yield}}/E_Y$, whereas for those with a high one the ratio $H_V/\sigma_{\text{Yield}}$ is lower and shows a complex dependence on $\sigma_{\text{Yield}}/E_Y$ and Poisson's ratio. This analysis was supported by experimental data for a variety of different materials, such as hard carbon and chromium steels, copper–beryllium, poly(methylmethacrylate), polystyrene, epoxy- and polyacetal resin and variety of glasses.[62,63] Based on these results it is obvious that the explanation of the correlation between the elastic modulus and hardness based on Eqs. (4) and (5) cannot be considered as a universal one and an alternative possibility should be considered, especially for the superhard nanocomposites.

In this section we shall show that the apparent, very high values of the elastic modulus (or more exactly the stiffness) as measured by the indentation technique on the super- and ultrahard nanocomposite coatings are due most probably to a high pressure under the indenter. Let us first briefly summarize which properties of the material determine the elastic moduli. The Young's elastic modulus E_Y is given by the second derivative of the bond energy E_b with interatomic distance x, i.e., to the curvature of the interatomic potential curve at the equilibrium interatomic distance x_0, Eq. (6) and Fig. 4(a):[2–4]

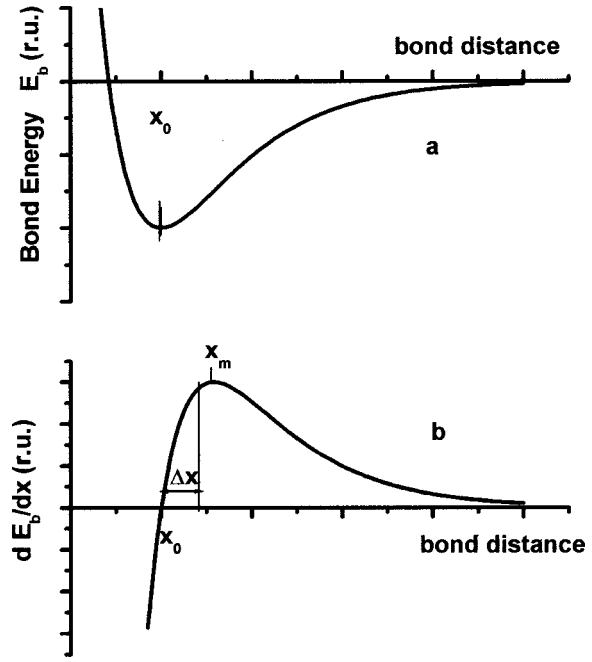

FIG. 4. Young's modulus corresponds to the curvature of the interatomic potential curve at the equilibrium position x_0 (upper curve). Upon compression, this "equilibrium" position decreases and the curvature (i.e., Young's modulus) increases. The first derivative of binding energy with bond distance is the restoring force when the interatomic bond length is changed due to applied stress.

$$E_Y = \left(\frac{d^2E_b}{dx^2}\right)_{x_0} \cdot x_0^2. \tag{6}$$

The larger the binding energy E_b and shorter the bond distance x_0, the larger the Young's modulus [Fig. 4(a)]. If a solid is subjected to compression, the bond distance decreases and the curvature of the potential curve, i.e., the elastic modulus, increases.

The bulk modulus B is equal to the reciprocal of the compressibility. It is given by the second derivative of the crystal energy U_C with dilatation, Eq (7):[64,65]

$$B = -\left(\frac{d(V/V_0)}{dP}\right)^{-1} = V_{\text{mole}}^2 \frac{\delta^2 U_C}{\delta V^2}. \tag{7}$$

In other terms, the bulk modulus is a measure of the increase of the crystal energy with a change of the volume imposed by an external hydrostatic pressure, Eq. (8):

$$U_C(V) = U_C(V_0) + \left(\frac{\delta U_C}{\delta V}\right)_{V_0} \cdot \delta V + \frac{1}{2}\left(\frac{\delta^2 U_C}{\delta V^2}\right)_{V_0} \cdot \delta V^2 + \cdots. \tag{8}$$

TABLE I. Examples of experimental values of the first derivative of bulk modulus with pressure.

Material	dB/dP	Reference
B_4C	4.26	74
$SrSi_2$	4.8	75
$EuSi_2$	4.3	75
$CaSi_2$	4.2	75
$BaSi_2$	3.9	75
Si	4.20–4.25	76, 77
Ge	4.81	77
Au	5.94	77
Ta	6.86	78
Fe	5.85	78
NaCl	5.88	77
KCl	4.67	77
MgO	4.8	79

Here V_0 is the molar volume at zero pressure and $U_C(V_0)$ is the crystal energy at equilibrium, i.e., $(\delta U_C/\delta V)_{V_0}=0$. Thus, the increase of the crystal energy upon hydrostatic pressure is given by the increase of the curvature of the potential surface in three dimensions in a way similar as in the simple, illustrative case of Young's modulus.[66–68] Therefore, elastic moduli are inherently associated with the crystal structure and nature of the chemical bonds of a given material.

The fairly linear increase of bulk modulus with pressure,[69] dB/dP, is due to the increase of the crystal energy with decreasing distances between the atoms, i.e., due to the increasing curvature of the interatomic potential surface[70] in a similar way as for the Young's modulus. That increase depends on the nature of chemical bonds and on the crystal lattice, but the values of the first derivative of B with P, $\delta B/\delta P$, are within a relatively small range of about 3–8 for the majority of materials, as summarized below.

Grover, Getting, and Kennedy[71] have shown that under compression, the logarithm of the isothermal bulk modulus of many metals increases almost linearly with the decrease of the specific volume $-\Delta V/V_0$ up to volume changes of 40%. The slope of these dependencies varied for different metals within the range of about 3 and 8. Rose calculated the higher order elastic constants for fcc metals, such as Cu, Ag, Al, and Ni and their pressure dependence $\partial c_{ij}/\partial P=A+2C\cdot P$.[72,73] The values of the constants A and C were between 5.00 and 5.45 and 0.005 and 0.11 (GPa^{-1}), respectively, for c_{11} and between 4.27 and 4.6 and 0.004 and 0.009 (GPa^{-1}), respectively for c_{12}. The corresponding constants A and C of bulk modulus $B=(c_{11}+2c_{12})/3$ varied from 4.53 to 4.9 and 0.004 to 0.010 (GPa^{-1}), respectively. This is in agreement with the experimental values within the accuracy of measurements as well as with the data for other materials (see Table I[74–79]) and recent theoretical work.[79–81]

Rose *et al.*[80] derived a universal zero-temperature equation of state which allowed them to calculate the first derivative of bulk modulus as a universal function of the ratio of the Wigner–Seitz atomic radius at equilibrium, r_{WSE}, to the width of the interatomic binding energy curve l, which corresponds to the anharmonicity of the crystal [Eq. (9)]. This expression yields theoretical values in a fairly good agreement with the experimental ones for a large number of solids (see Table III in Ref. 80). In a more recent article these authors extended their consideration also to interfaces[81]

$$\left(\frac{\partial B}{\partial P}\right)_T=1+\frac{2.3}{3}\frac{r_{WSE}}{l}. \tag{9}$$

Thus, the pressure dependence of elastic moduli can be fairly well approximated by a proportionality (10) with A being between about 3 and 8:

$$B(P)\cong B(0)+A\cdot P. \tag{10}$$

The Young's moduli and shear moduli also show an increase with pressure. Manghnani, Wang, and Zinin[74] reported the values of the first derivative of 3.85 and 1.1 for Young's modulus and shear modulus of B_4C, respectively. The approximate dependence of the elastic shear modulus G on pressure in ionic solids, $G(P)\cong G(0)+0.5P$, was elaborated by Kelly, Thyson, and Cottrell[82] and discussed in some detail by Argon.[83]

The effective modulus measured by the load-depth sensing indentation technique is calculated from the linear part of the unloading curve and corrected for the possible elastic deformation of the diamond indenter according to the original Sneddon analysis.[84] More recent work has, however, shown that the original formula used for the evaluation of the elastic modulus is too simplified in real indentation measurements.[85,86] Moreover, the assumption of a ''rigid punch'' used in Sneddon's calculation (see third line in Ref. 84) is violated for super- and ultrahard nanocomposites. Thus, the effective elastic modulus measured by the indentation is a complex function of the compression, shear, and tensile components of the elastic tensor and the corresponding moduli.

Let us consider the possible effect of the pressure induced by the indenter during the measurement on superhard coatings. As already pointed out by Tabor,[54] indentation Vickers hardness H_V is a direct measure of the average pressure P under the indenter

$$H_V(\mathrm{GPa})\approx 0.927P(\mathrm{GPa}), \tag{11}$$

where the constant 0.927 accounts for the difference between the projected area of the indentation and the exact area of the contact between the indenter and the material.[87] Under conditions of yielding (plastic deformation) of the material being measured[88] when the yield pressure is essentially constant and independent of the applied load L, the pressure under the indenter

$$P\approx\frac{H_V}{0.927}=\frac{L}{A}, \tag{12}$$

where A is the projected area of the remaining indentation.[54] The higher the hardness the smaller the area A and the higher the average pressure under the indenter. Of course, the distribution of the pressure under the indenter is complex and was calculated only for several simple cases.[54,61,89] Never-

theless, it is clear that the higher the hardness the higher the pressure under the indenter under the maximum applied load where the elastic modulus is evaluated from the unloading curve.

A direct experimental evidence of high pressure under the indenter is the presence of structural phase transitions induced by the high hydrostatic pressure during the indentation. An example *par excellence* is the semiconductor-to-metal transition in silicon which commences at about 11.3 and is completed at 12.5 GPa.[76] This transition is observed upon indentation with a Vickers indenter at an applied load of about 30–40 mN and it is best seen on the unloading curve.[90] It is accompanied by a strong decrease of electric resistivity of silicon within the indentation area (see Ref. 91 and references therein). Gridneva, Milan, and Trefilov reported the semiconductor-to-metal transition upon indentation in Si, Ge, InSb, and GaAs and have shown that the pressure under the indenter at which this transition occurs determines the measured hardness of the given material.[92]

Considering two materials of a similar chemical composition but different hardness $H_1 < H_2$ which, upon the same load show indentation areas $A_1 > A_2$, the corresponding pressures under the indenter within the linear part of the unloading curve will be

$$P_1(\propto L/A_1 \propto H_1) < P_2(\propto L/A_2 \propto H_2). \tag{13}$$

which yields the proportionality $P \propto H$. Therefore the ''elastic moduli'' measured for these materials by the indentation at the same load will correspond to a larger pressure in the compressed zone under the indenter for the harder material than for the softer one. Considering the pressure dependence of elastic moduli mentioned above the measured complex indentation elastic modulus B_{ind} will increase with the hardness of the material

$$B_{\text{ind}} \approx B(0) + C_{\text{ind}} \cdot H_{\text{plastic}}, \tag{14}$$

where $B(0)$ is the extrapolated elastic modulus at zero pressure and C_{ind} is close to the value of the first derivative of the elastic modulus with pressure. The exact value of the constant C_{ind} depends on the exact mode of the plastic deformation which determines the relevant elastic moduli. Materials which deform plastically by multiplication and movement of dislocations are expected to show a dependence of the measured B_{ind} on H_{plastic} corresponding to that of the shear modulus on pressure,[55,56] whereas ceramics and superhard nanocomposites are likely to show a dependence more resembling that of the bulk modulus. This has visual confirmation in the former by the plowed-up material around the indentation and an absence of it in the latter.

Figure 5 shows experimental data obtained for a range of materials including various diamond coatings and super- and ultrahard nanocomposites.[48] The relatively large scatter of the data is due probably to different modes of the plastic deformation and different pressure dependence of the elastic moduli.

In order to obtain the dependence of the ''indentation elastic modulus'' for similar ceramics-like materials, we compare in Fig. 6 *nc*-TiN/*a*-Si_3N_4/*a*- and *nc*-$TiSi_x$ nano-

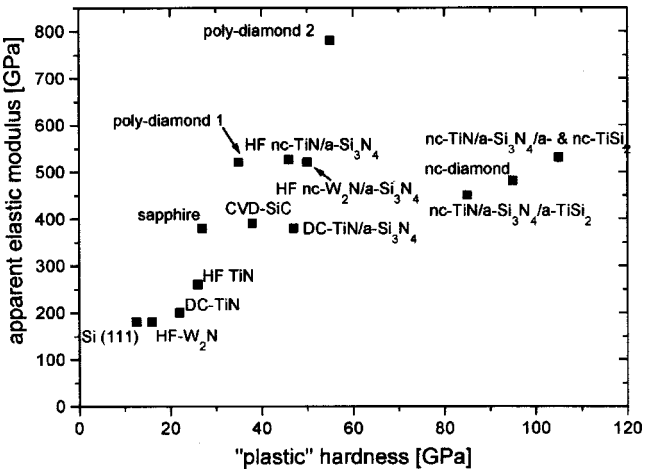

FIG. 5. Correlation between the elastic modulus measured by the load-depth sensing technique and the corresponding plastic hardness for various materials and coatings (adapted from Ref. 48). Notice the good agreement of the data for sapphire (α-Al_2O_3) with those reported by Oliver and Pharr (see Ref. 95).

composites which were prepared under similar conditions and which differ only by the fraction of the Si_3N_4 and $TiSi_x$, the main phase being TiN.[47–49,93,94] Let us emphasize that the total silicon content in these super- and ultrahard nanocomposites varied only between 0 and about 20 at. %. The main influence on the hardness is due to the coverage of the nanocrystals with Si_3N_4.[39,47,49] As is apparent, the measured values of the elastic moduli of these coatings vary fairly proportionally with the hardness, the proportionality factor being approximately 3.8, i.e., within the range of the values of first derivative of bulk modulus with pressure for a major-

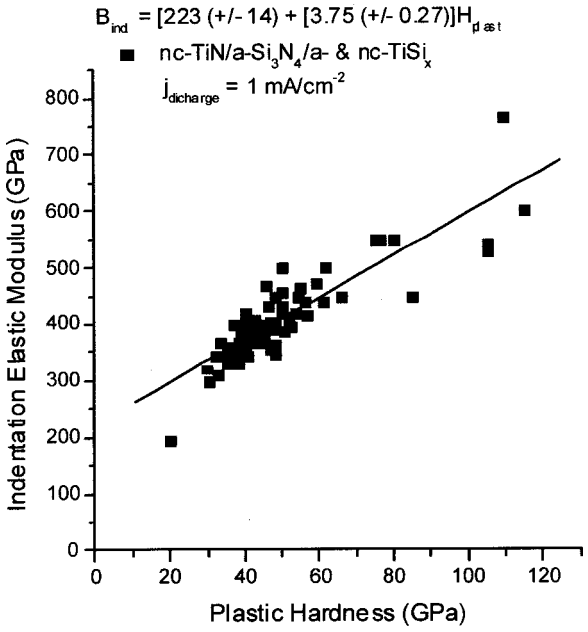

FIG. 6. Dependence of the elastic modulus $E_Y/(1-\nu^2)$ measured by the load-depth indentation technique for a series of *nc*-TiN/*a*-Si_3N_4/*a*- and *nc*-$TiSi_x$ films containing a variable fraction of the phases with total Si content $\leqslant$ 20 at. %.

ity of solids. A similar relationship was reported for other superhard nanocomposite coatings.[13–16] This lends a strong support to the suggested enhancement of the indentation elastic moduli of the super- and ultrahard nanocomposites by the high pressure induced under the indenter during the measurement.

In their original work Doerner and Nix[45] and Oliver and Pharr[95] compared the values of elastic moduli measured by the indentation method with those reported in the literature (data obtained from the isostatic compressibility and/or ultrasonic wave propagation measurements) for Al, quartz, soda-lime glass, sapphire, fused silica, and tungsten and concluded that there is a good agreement. However, for the hardest material, sapphire, measured by these authors the value of the indentation elastic modulus is about 10% larger than that from the literature. Indeed, for relatively soft material with hardness below about 10 GPa and elastic modulus of 200–400 GPa one would expect the enhancement of the indentation elastic modulus due to the pressure under the indenter to be within the scatter of the literature data because, as already mentioned, the first derivative of the bulk modulus with pressure is typically between 3 and 7. The pressure enhanced elevation of elastic constants becomes significant only with hardness increasing significantly above 20 GPa as in the case of the superhard nanocomposites. Therefore, values of apparent indentation elastic moduli in the range of diamond or even higher for materials which, based on the fundamental considerations stated above must have much lower values, are artifactially elevated due to the high pressure. It is unnecessary as well as improper to evoke other possible explanations, such as the increase of the modulus due to the interface incoherence strain hardening.[96–99]

In order to obtain exact values of the elastic moduli, appropriate techniques should be used, such as isostatic compression combined with *in situ* x-ray diffraction (XRD) for bulk modulus, cantilever technique for the tensile measurements, and surface acoustic waves on specially prepared specimens for Young's modulus. It would also be interesting to determine, by means of an appropriate specimen preparation and measurements, the shear modulus because it should show the best correlation with the plastic hardness provided there is a similarity in the mechanism of plastic deformation in these nanocomposites and in the ordinary materials.[55,56,100,101] Such a measurement is ideally done by means of a torque-twist experiment on coated isotropic circular filament such as fused silica.

B. Hardness, elastic recovery and possible mechanism of plastic deformation

1. Nanostructure, stress concentration factor, and hardness

The smaller the dissipated energy of the plastic deformation (area between the loading and unloading curve in Fig. 1) and larger that of the elastic one (area between the unloading curve and axis *y*) the larger the hardness and elastic recovery of the material. Conventional hard materials with $H_V \approx 20-30$ GPa sustain a relatively small strain of $<0.1\%$ within the region of elastic deformation and undergo brittle fracture when this limit is exceeded.[2–5] Only specially toughened modern ceramics show a somewhat higher elastic recovery.[102,103]

In contrast, the superhard nanocomposites *nc*-M_nN/*a*-Si_3N_4 (M=Ti, W, V) with hardness of about 50 GPa have elastic recovery in the range of 80%[15] which increases to more than 90% for the ultrahard nanocomposites of *nc*-TiN/*a*-Si_3N_4/*a*- and *nc*-$TiSi_2$ [see Fig. 1(b) and Refs. 47–49]. In the case of the sample shown in Fig. 3(a) the 6.1 μm coating was, at the highest applied load, pressed about 2 μm into the soft steel substrate without showing any cracking or delamination observable on the surface by SEM (certainly causing a broader level of plastic deformation in the steel substrate but also a tensile strain in the coating at the interface probably exceeding 25%, depending on the level of dispersal of the plastic flow in the substrate). The understanding of this unusual behavior is an important challenge to be discussed in this section. The second, related question of more fundamental importance concerns the nature of the plastic deformation in the nanocomposites with crystallite size of 3–6 nm in which crystal plasticity (due to dislocations) cannot develop. The third question to be discussed is the origin of the high hardness. All these questions are integrally related to the scale of the nanocomposites and their thermal stability.

Because the most complete information regarding the composition and nanostructure is available for the *nc*-TiN/*a*-Si_3N_4 and *nc*-TiN/*a*-Si_3N_4/*a*- and *nc*-$TiSi_2$ nanocomposites we shall now concentrate on these systems. Similar conclusions will also apply for other superhard nanocomposites which display a well developed, strong segregation and spinodal decomposition, such as *nc*-W_2N/*a*-Si_3N_4, *nc*-VN/*a*-Si_3N_4,[15,16] *nc*-TiN/BN,[104] *nc*-TiN/AlN [or $(Ti_{1-x}Al_x)N/Al_{1-\delta}Ti_\delta)N$], $(Ti_{1-x}Al_x)N$/*a*-Si_3N_4,[105] *nc*-M_nN/*a*-C:N (M=Ti, Zr,...)[106–110] and others.

In our earlier publications it has been shown that the maximum hardness is achieved when the crystallite size reaches 3–4 nm and the concentration of Si_3N_4 of about 16–20 vol. % which corresponds to the percolation threshold in a three-dimensional network.[6,14–16] As an explanation of this behavior it was suggested that the nonpolar Si_3N_4 is wetting the polar (high energy) surfaces of the transition metal nitride nanocrystals thus decreasing the energy of the interface, which of course always represents a positive, i.e., destabilizing contribution to the total free energy of the system. The same was also found for the ternary and quaternary ultrahard nanocomposites *nc*-TiN/*a*-Si_3N_4/*a*- and *nc*-$TiSi_2$[47,49] and evidence is growing which shows that this is generally valid for other superhard nanocompsites which show a high thermal stability.[6,39,132] (See *Note Added in Proof.*)

The XRD and high resolution transmission microscopy (HRTEM) studies have shown that in the nanocomposites with the highest hardness, the TiN nanocrystals are randomly oriented and have fairly regular equiaxed shapes.[111] Similar results were recently found also for the *nc*-$(Ti_{1-x}Al_x)N$/

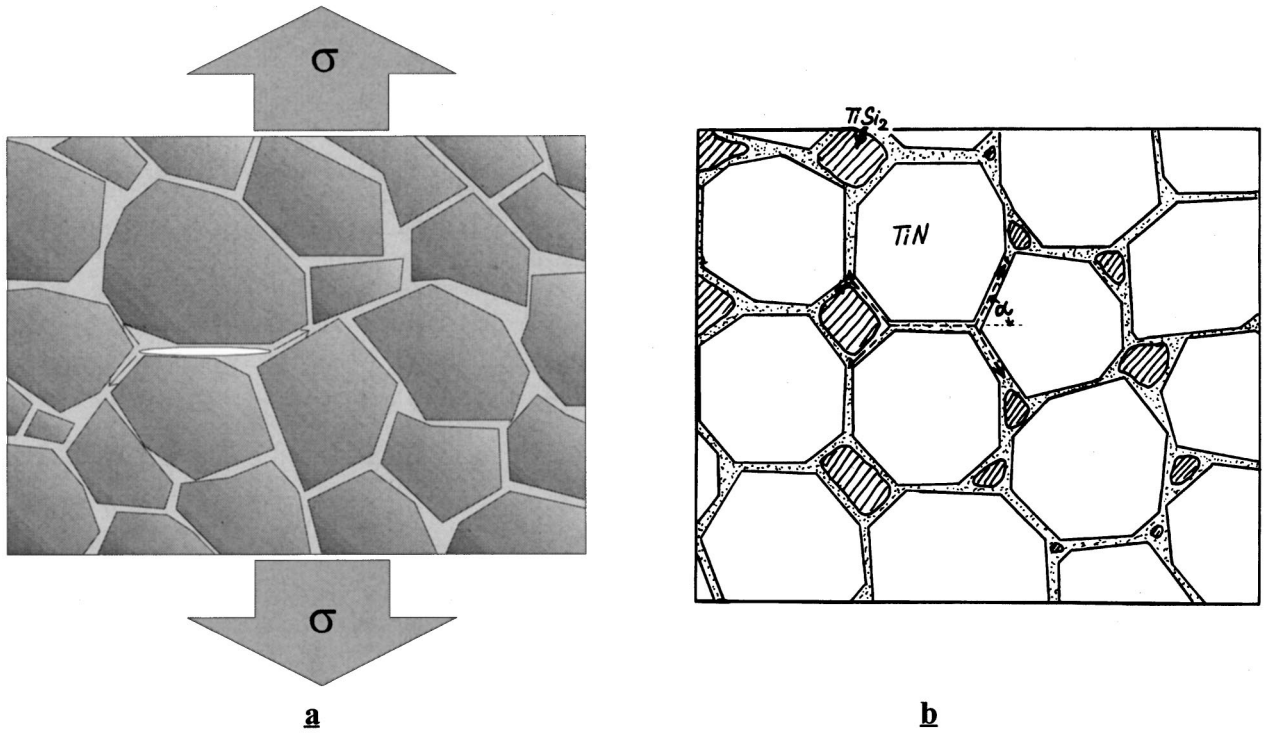

FIG. 7. (a) Nanostructure of the ultrahard nc-TiN/a-Si_3N_4 nanocomposites, (b) nanostructure of ultrahard nc-TiN/a-Si_3N_4/a- and nc-$TiSi_2$.

a-Si_3N_4 and nc-TiN/a-Si_3N_4/a-$TiSi_2$ nanocomposites.[39] Summarizing all these data, the nanostructure of the superhard nc-TiN/a-Si_3N_4 nanocomposites is schematically shown in Fig. 7(a) with a nanocrack in the process of forming under an applied tensile stress (and possibly also in response to internal misfit stresses, see also Refs. 15, 16, and 49). The ultrahard nanocomposites nc-TiN/a-Si_3N_4/a-$TiSi_2$ ($H_V \geqslant 80$ GPa) have a similar nanostructure with the third phase a-$TiSi_2$ in the a-Si_3N_4 interfacial layers of the nanocrystals and also filling the remaining space in the interfacial multijunction points.[112] Notice, that the maximum hardness in these nanocomposites is obtained when the content of a-$TiSi_2$ amounts to about 4–5 mol %.[39,47–49] When the total silicon content exceeds about 10 mol %, nanocrystalline $TiSi_2$ phase precipitates with a crystallite size of about 3 nm, i.e., smaller than that of the nc-TiN which, in this case, have sizes of about 7–10 nm for nanocomposites reaching hardness of $\geqslant$80 GPa. The ultrahard nc-TiN/a-Si_3N_4/a- and nc-$TiSi_2$ nanocomposites whose hardness exceeds 100 GPa have a total silicon content of about 15–20 at. %.[47–49] Their nanosctructure is schematically shown in Fig. 7(b).

As already mentioned, the 3–10 nm size nanocrystals cannot accommodate any crystal plasticity for obvious reasons nor any other form of flaw. Therefore, their strength will approach the ideal one which is of the order of about 10% of the shear modulus.[2–5] This means that the existence of transgranular cracks is not likely. Consequently, initiation and growth of intergranular cracks propagating within the interfacial component, i.e., the grain boundaries of the nanocrystals, ''glued'' together by a layer of atomic dimensions of Si_3N_4,[15,16,39] should be the most probable fracture mechanism of these materials. The actual behavior is likely to be more complex as we describe below.

In the first approximation the stability of a material against catastrophic crack growth is described by the Griffith thermodynamic criterion

$$\sigma_c = k \cdot \sqrt{\frac{\gamma \cdot E_Y}{a}}, \tag{15}$$

where σ_c is the critical applied stress which causes the catastrophic crack growth, E_Y is the Young's modulus, γ is the surface free energy of the material, $2a$ is the size of the crack[2–5] and k is a constant which depends on the crack shape. Because in the randomly oriented nanocomposites the size of such cracks can only be a fraction of the crystallite size, i.e., of 1–2 nm, the stress concentration factor of an atomically sharp crack is very low and the critical stress for the crack growth approaches extremely high values.[49] This can be more illustratively seen by considering a simple formula for the stress concentration factor of a penny shaped nanocrack

$$\frac{\sigma_{\text{tip}}}{\sigma_{\text{applied}}} = 1 + 2\sqrt{\frac{a}{\rho}} \tag{16}$$

which is the ratio of the stress acting at the tip of the crack (of radius ρ and a size of $2a$) to the applied stress.[3,5] The larger the crack and smaller the tip radius the larger the stress concentration factor. The smallest possible tip radius corresponds to the interatomic distance, i.e., 0.2–0.3 nm. For microcracks of the size of 100–1000 nm in a conventional ceramic the stress concentration factor is about 37–140. This

means that the applied stress which is about 37–140 times smaller than the theoretical one is sufficient to cause catastrophic crack growth. On the other hand, for a nanocrack of the size of 1–2 nm the stress concentration factor decreases to about 2–4, i.e., the stress needed to propagate the crack approaches a significant fraction of the ideal strength. Although these considerations are quite simplified, they clearly show that the initiation (''opening'') of cracks in nanocomposites with crystallite size of 3–8 nm and having very thin, strongly bonded interfaces requires very high applied stress. Much of computer simulations with large computers using appropriate interaction laws have shown that the Griffith relation should be accurate in this nanoscale range.[101]

Because only the stress component perpendicular to the crack plane causes the crack growth, the first nanosized cracks to be considered as operating under an applied load are those within the interfaces perpendicular to the direction of the applied tensile stress. For simplicity we consider here only uniaxial stress with components pointing up and down in Fig. 7. After the opening, the nanocrack can grow within that plane only up to the nearest obstacle, such as the neighbor nanocrystal, where it has to undergo deflection and branching. Upon the deflection the component of applied stress which is perpendicular to the crack plane decreases as $\cos\alpha$ where α is the angle between the applied uniaxial stress and the normal to the plane of the deflected crack or just the angle of the crack deflection. Furthermore, the crack deflection occurs within a three-dimensional network, leading to corresponding branching which further increases the total length of the crack and corresponding decrease of the stress concentration factor. Last but not least, planar interfaces such as shown in the schematic structure of Fig. 7 are unlikely in the real materials where faceting of the surfaces of the neighbor crystallites are common. Thus, one can easily see that for a nanocomposite with grain size of a few nanometers and the thickness of the interface phase (e.g., Si_3N_4) of about 1 ML the deflected and branched crack will stop within a small distance of the order of 1 nm unless the applied stress will be significantly increased which, however, would lead to catastrophic fracture. For these reasons, contained fracture of the nanocomposites due to a formation and stable growth (percolation) of nanocracks is unlikely[113] and other mechanisms of inelastic[114] deformation should be responsible for the high hardness and elastic recovery found in these materials as discussed in the following sections.

2. Elastic recovery and reversible stored elastic energy

It is interesting to estimate the energy of elastic deformation actually measured in the indentation experiments. Figure 1(b) shows a typical example of an indentation into 3.5 μm thin ultrahard coating with elastic recovery of about 94% which shows energy of elastic deformation of about 1×10^{-8} J.[115] Similar values can be also estimated from a number of indentations performed in other superhard nanocomposite coatings (see, e.g., Fig. 1 in Ref. 49). Assuming the total area of the deformation under the maximum applied load of 0.07 N [Fig. 1(b)] to be about four times the area of the permanent, plastic deformation as obtained from the load-depth sensing indentation measurements and SEM micrographs [see Fig. 3(c) and Ref. 47] yields the elastic energy density of about 3×10^{8} J m^{-3},[116] and finally the specific elastic energy of about 3 kJ mole^{-1}.[117]

The elastic energy U_{el} of a solid is given by Eq. (17) where B is the bulk modulus (of about $\leqslant$500 GPa) and $(\Delta V/V)_{\mathrm{el}}$ is the true elastic dilatation

$$U_{\mathrm{el}}=V_{\mathrm{mole}}\cdot\frac{B}{2}\cdot\left(\frac{\Delta V}{V}\right)_{\mathrm{el}}^{2}. \tag{17}$$

Assuming as an upper limit for the elastic dilatation of about 1% (i.e., much higher than what is typically found for conventional hard materials) and $V_{\mathrm{mole}}\approx10$ cm^3 (10^{-5} m^3) the elastic energy density of the order of 0.5 kJ/mole results. This value is much smaller than the above estimated energy density as measured by the indentation. In the following we discuss the possible explanations and suggest further more detailed future studies which should be done in order to verify them and decide which is the dominant one.

The first possibility may be that the elastic deformation extends over a much larger volume than what was assumed above. This would require that the lateral area of elastic deformation should be more than 20 times larger than the measured area of the remaining plastic deformation and that the elastic strain density does not decrease very rapidly with increasing distance from the point of indentation, which is just the opposite as generally found. Consequently, the elastic and plastic deformation of the steel substrate has to be involved and considered in the analysis. This may be done by means of a sophisticated finite element analysis which is beyond the scope of this article.[133]

The other possibility is that the nanostructured superhard coatings being discussed here may indeed sustain a high strain approaching 10% without undergoing plastic deformation. This is beyond the well known behavior of conventional hard materials, but it cannot be completely ruled out for the superhard nanocomposites for the following reasons: In the nanostructured materials with 3–5 nm small, equiaxed nanocrystals the dimensions of the initial flaws induced by the high applied stress are at the scale of $\leqslant$1 nm (see above). This means that the tips of cracks or any other small voids formed, e.g., during the visco-elastic flow under the very high applied stress, remains at the scale comparable with the interatomic bond length. It is well known that the rupture strain of interatomic bond can reach up to 20%. In order to clarify this question, advanced first principles computer modeling of the elastic behavior of such complex nanostructure are needed.

A third, closely related possibility is a reversible nonlinear flexing (a ''partial opening and closure'' of interplanar spacing) between nanocrystallites. Consider the dependence of the interatomic binding energy on interatomic distance as shown in Fig. 4(b) for $x\geqslant x_0$. The dependence of the first derivative of E_{binding} with x is shown in Fig. 4(b) and the flexing is schematically illustrated in Fig. 8. The relationship

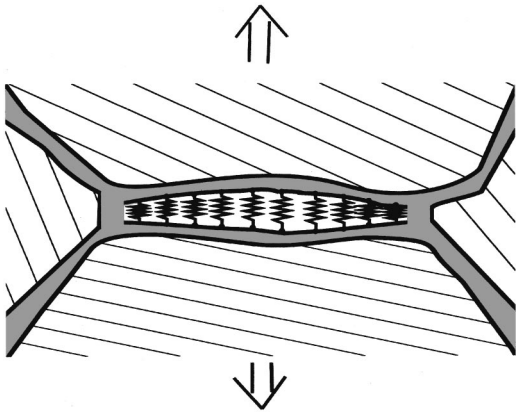

FIG. 8. Schematics of reversible flexing where the bond length dilatation can exceed 10%–20% of the equilibrium bond length.

in Fig. 4(b) for $x > x_0$ is called ''fundamental decohesion curve.'' The first derivative of the binding energy with distance, dE_b/dx is the ''restoring'' force acting against the applied tensile stress. The elastic energy due to the reversible flexing of the bonds across the interface by Δx is given by the area under the curve dE_b/dx between x_0 and Δx in Fig. 4(b). Whenever the elastic strain energy associated with the elastic deformation of the attached nanocrystals is less than the above energy of the flexing of the bonds across the interface, the system will be reversible.[118] Therefore the energy of flexing will be fully recovered upon unloading. In such a way the flexing will show as a reversible plasticity, such as that associated with martensitic transformations and twinning.[3,4,119] Considering the fundamental decohesion curve, a simple estimate shows that the energy which is reversibly stored in the nonlinear flexing can exceed that of elastic deformation by a large factor, but experimental work (HRTEM) and finite element modeling which can account for the nonlinearity of the flexing is required for more exact calculations.

3. Plastic deformation

Experimental evidence shows clearly that there is also an irreversible plastic deformation associated with the indentation which must come from localized shear events most probably within the intercrystalline ''amorphous'' component, akin to the local shear transformations in amorphous materials discussed by a number of workers (e.g., Refs. 120–122) which, if spatially isolated will result in a ''homogeneous'' deformation. If of a percolative nature, such deformation will produce localization in the form of shear bands as observed in the work of Bull, Page, and Yoffe[123] and others.[124] Because no such ''deformation bands'' were observed in a large number of SEM micrographs from our nanocomposites (e.g., Fig. 3) we conclude that the individual shear events have remained spatially isolated for reasons discussed by Bulatov and Argon in Ref. 125. It will be very difficult to prove this experimentally by means of high resolution TEM or other techniques in view of the nanostructured nature of the films, their high strength, and relatively small thickness, not to mention the possible reversible features of the response.

Another possibility worth considering to explain the plastic response could be densification transformations due to the high pressure under the indenter such as that observed in silicon and other materials mentioned above, in the high pressure modifications of silica and others. This might be observable in high resolution transmission electron microscopy if the density increase will be similar to that found for the high pressure phases (e.g., 4.4 g/cm^3 for Stishovith as compared to 2.6 g/cm^3 for α-quartz).

C. Issue of apparent high fracture toughness

Fracture toughness is the ability of a material to resist fracture due to catastrophic crack growth. The presence of a critical crack [see Eq. (15)] is a statistical possibility which depends, among other factors, on the material preparation. The fracture toughness is conventionally measured by a critical stress intensity factor K_{IC} defined as

$$K_{IC} = \sigma \cdot (\pi \cdot a)^{1/2}. \tag{18}$$

This critical value is governed by material specific parameters, such as surface free energy γ, Young's modulus E_Y, and Poissons ratio ν, $K_{IC} = \sqrt{2E_Y \cdot \gamma/(1-\nu^2)}$ for brittle fracture. It describes the stress σ needed to propagate a crack of the size $2a$. The larger K_{IC}, the larger the fracture toughness. The most convenient way of measuring the critical stress intensity factor in ceramics[102] and thin films[126,127] is by indentation which, when performed in bulk material at sufficiently high load, results in the formation of radial cracks emanating from the indentation site. Pharr[42] has shown that Vickers indenter may need a high threshold for the crack initiation because of its geometry which results in a relatively small stress at the edges of the pyramid. From the dependence of the crack length on the applied load, the critical stress intensity factor K_{IC} is evaluated. However, in order to exclude the effect of the substrate in the case of coatings which may falsify the results (e.g., singularities on the substrate surface may initiate a ''subcritical'' crack to grow) the length of the cracks should be much less than the thickness of the film.[127] This condition is difficult to meet even for 10–20-μm-thick coatings.

Our attempt to measure the critical stress intensity factor on the superhard nc-TiN/a-Si_4N_4 and ultrahard nc-TiN/a-Si_3N_4/a- and nc-$TiSi_2$ coatings was so far not successful because radial cracks were not found even at very high loads of 1000 mN applied to 3.5 μm thin films, where the coatings were pressed 5 μm into the soft steel substrate (see Fig. 3 and Refs. 6 and 47). Since the compressive stress in these coatings of $\leqslant 1$ GPa is fairly low, the possibility of falsification of the measurements due to a high compressive residual stress can be ruled out.

On the basis of available data the absence of radial cracks after the indentation is due most probably to a high stress threshold for crack initiation because of the extremely small size and low concentration of possible flaws in the nanocom-

posites which is the result of the ''self-organization'' of their nanostructure during the deposition, phase segregation and spinodal decomposition[39] as outlined in the Introduction. Considering Eq. (18) for a micro- (crystallite size $d \geqslant 1000$ nm) and nanocrystalline ($d < 10$ nm) materials of the same composition it is obvious that a more than ten-times larger applied stress will be needed to propagate cracks in the nanocomposite than in the microcrystalline material even if both would have the same stress intensity factor. The very high resistance of the superhard nanocomposites against crack formation can be understood in a simple and natural way. From the practical point of view, the absence of the cracks is encouraging property of the super- and ultrahard nanocomposites applied to ductile substrates.

III. FURTHER CONSIDERATIONS AND OUTLOOK

The ideas outlined in this article provide a simple basis for the overall understanding of the unusual combination of the mechanical properties of the nanocomposites which should be elaborated in more quantitative models accounting also for further effects which we have neglected so far. Among these, random strain which arises due to mismatch of thermal expansion of the different phases as well as to their lattice mismatch and random orientation of the nanocrystal should be considered. Such effects are believed to play an important role in toughening of cemented carbide[128] as well as in modern ceramics, such as SiC reinforced Al_2O_3 matrix composites where few vol.% of nanocrystalline SiC significantly increase the strength and, possibly, also toughness.[102,129,130] However, in spite of more than ten years research, the mechanism of strengthening in the SiC reinforced Al_2O_3 ceramics is still under debate and by far not fully understood. Recently, Derby suggested, that the observed improvement of the mechanical properties of this material may be a simple consequence of a lower density of flaws present in that material after its processing.[103]

The latter suggestion is worth considering as a possible explanation of the high hardness and apparent toughness of our superhard nanocomposites. The experimentally documented finding that the *nc*-TiN/*a*-Si_3N_4 nanocomposites do not show any recrystallization or other kind of structural relaxation upon annealing to a temperature exceeding half of the decomposition point of Si_3N_4 and TiN, i.e., much higher than the deposition temperature of 550 °C[13–16,38,47,49] suggests that these nanocomposites may be fairly free of flaws. Furthermore, the development of the morphology from the columnar for pure transition metal nitrides (TiN, W_2N) towards a dense, isotropic one of the self-organized *nc*-M_nN/*a*-Si_3N_4 nanocomposites with the optimum composition[15] also indicates, that there is some chemistry operating in these systems which stabilizes their nanostructure and makes it fairly free of flaws. A similar self-organization was also observed for some other superhard nanocomposites (see Ref. 6 and references therein). This is further supported by the recent results which show that such coatings prepared by combined reactive sputtering and plasma CVD as well as the *nc*-$(Ti_{1-x}Al_x)N$/*a*-Si_3N_4 nanocomposites deposited by means of vacuum arc evaporation[37,38,105] under conditions which do not allow to achieve the development of the optimum nanostructure show an increase of the hardness upon annealing due to structural relaxation which is observable by XRD.[131]

So far, we have discussed binary systems, such as *nc*-TiN/*a*-Si_3N_4. Obviously, the presence of a third (e.g., *a*-$TiSi_2$) and fourth (*nc*-$TiSi_2$) phase which introduce random microstrain due to thermal dilatation and incoherency lattice mismatch may further increase the strength, hardness, and possibly toughess of such ternary and quaternary nanocomposites. The ultrahardness of $H_V \geqslant 80$ GPa in *nc*-TiN/*a*-Si_3N_4/*a*-$TiSi_2$ and $H_V \geqslant 100$ GPa in *nc*-TiN/*a*-Si_3N_4/*a*- and *nc*-$TiSi_2$ is probably associated with these effects. However, in view of the complexity of these systems and the associated problems regarding the possible contributions of the different potentially ''hardening'' and ''toughening'' mechanisms (see, e.g., Refs. 102, 103, 129, and 130) any attempt to elaborate these ideas in more detail would be, at this stage, too speculative. Most probably, various mechanisms of strengthening and possibly also toughening are active simultaneously which results in a multiplication of strengthening and toughening effects.[102] All these observations represent a challenge for first principle theoretical studies.

IV. CONCLUSIONS

It was shown that the unusual combination of the mechanical properties of the superhard and thermally surprisingly stable nanocomposites can be understood in terms of conventional fracture physics and mechanics scaled down to the size of the crystallites of a few nanometers which are glued together by a few tenths of nanometer thin amorphous layer with a high adherence to the surface of the crystallites. In such a nanostructure the dislocation activity is absent and the stress concentration factor on the tip of a 1–2 nm small nanocrack is very small. Consequently, the superhardness of $\geqslant 40$ GPa which exceeds that of the rule of mixtures results. The high resistance of the nanocomposites against crack formation upon a very high indentation load and strain exceeding 10% is a simple consequence of the small stress concentration factor and a low concentration of flaws in these self-organized nanocomposites which are formed due to spinodal decomposition. The very high values of elastic modulus measured by the indentation on such films with hardness exceeding 50 GPa is most probably due to a very high pressure within the region under the indenter. Several open problems are addressed and the way towards their solution briefly discussed.

Note Added in Proof: Recently we have shown that also for the system *nc*-TiN/*a*-BN the maximum hardness is obtained at the percolation threshold when the surface of the TiN nanocrystals is covered by about one monolayer of amorphous boron nitride.[132] We could also show that the super- and ultrahard nanocomposite can sustain a large tensile stress of 10 to 40 GPa, i.e., their tensile strength reaches a significant fraction of the ideal decohesion strength.[134,135]

Such a high tensile strength was reported only for thin whiskers and freshly drawn silica fibers[2] but our nanocomposites display a much larger reversible (elastic) strain.[135]

ACKNOWLEDGMENTS

The authors would like to thank the co-workers at TU Munich for fruitful collaboration with the sample preparation and characterization. This work has been supported in part by the NATO Science for Peace Programm SfP 972379, by the European Community under research Project NACODRY, German Science Foundation, and within a DURINT Program under Grant No. N00014-01-1-0808.

[1]This definition is suggested because the hardness of diamond varies between about 70 and 90 GPa.
[2]A. Kelly and N. H. MacMillan, *Strong Solids*, 3rd. ed. (Clarendon, Oxford, 1986).
[3]R. W. Hertzberg, *Deformation and Fracture Mechanics of Engineering Materials*, 3rd ed. (Wiley, New York, 1989).
[4]*Physical Metallurgy*, edited by R. W. Cahn and P. Haasen (North Holland, Amsterdam, 1996).
[5]T. L. Anderson, *Fracture Mechanics* (CRC, Boca Raton, FL, 1996).
[6]S. Veprek, J. Vac. Sci. Technol. A **17**, 2401 (1999).
[7]J. S. Koehler, Phys. Rev. B **2**, 547 (1970).
[8]S. A. Barnet, in *Physics of Thin Films, Vol. 17, Mechanic and Dieletric Properties*, edited by M. H. Francombe and J. L. Vossen (Academic, Boston, 1993), p. 2.
[9]S. A. Barnet and A. Madan, Phys. World **11**, 45 (1998).
[10]X. Chu and S. A. Barnet, J. Appl. Phys. **77**, 4403 (1995).
[11]P. M. Anderson and C. Li, Nanostruct. Mater. **5**, 349 (1995).
[12]L. Shizhi, S. Yulong, and P. Hongrui, Plasma Chem. Plasma Process. **12**, 287 (1992).
[13]S. Veprek, S. Reiprich, and L. Shizhi, Appl. Phys. Lett. **66**, 2640 (1995).
[14]S. Veprek and S. Reiprich, Thin Solid Films **268**, 64 (1996).
[15]S. Veprek, M. Haussmann, and S. Reiprich, J. Vac. Sci. Technol. A **14**, 46 (1996).
[16]S. Veprek, M. Haussmann, S. Reiprich, L. Shizhi, and J. Dian, Surf. Coat. Technol. **86–87**, 394 (1996).
[17]The Vickers hardness values from Refs. 18–20 are: $H(TiN)\approx 21$ GPa, $H(VN)\approx 15$ GPa, $H(W_2N)\approx 17$ GPa, $H(Si_3N_4)\approx 17$ GPa.
[18]L. E. Toth, *Transition Metal Carbides and Nitrides* (Academic, New York, 1971).
[19]G. V. Samsonov, *Nitrides* (Naukova Dumka, Kiev, 1969) (in Russian).
[20]H. Holleck, J. Vac. Sci. Technol. A **4**, 2661 (1986).
[21]J. Musil, P. Zeman, H. Hruby, and P. H. Maryhofer, Surf. Coat. Technol. **120-121**, 179 (1999).
[22]M. Misina, J. Musil, and S. Kadlec, Surf. Coat. Technol. **110**, 168 (1998).
[23]J. Musil and P. Zeman, Vacuum **52**, 269 (1999).
[24]J. Musil, I. Leipner, and M. Kolega, Surf. Coat. Technol. **115**, 32 (1999).
[25]J. Musil, Surf. Coat. Technol. **125**, 322 (2000).
[26]P. Karvankova, H. Männling, and S. Veprek, Surf. Coat. Technol. **146-147**, 280 (2001).
[27]T. Y. Tsui, W. C. Oliver, and G. M. O. Pharr, J. Mater. Res. **11**, 752 (1996).
[28]A. Bolshakov, W. C. Oliver, and G. M. Pharr, J. Mater. Res. **11**, 760 (1996).
[29]W. Herr and E. Broszeit, Surf. Coat. Technol. **97**, 335 (1997).
[30]J. Musil, S. Kadlec, J. Vyskocil, and V. Valvoda, Thin Solid Films **167**, 107 (1988).
[31]V. Valvoda, R. Cerny, R. Kuzel, J. Musil, and V. Poulek, Thin Solid Films **158**, 225 (1988).
[32]Let us emphasize that the annealing experiments are a reliable check for the correct value of the intrinsic hardness only if the mismatch of the thermal dilatation of the film and substrate is sufficiently small, because otherwise large stress in the thin film may build up upon the cooling of the sample to room temperature. Depending on the sign of the thermal mismatch, the stress in the film can be either compressive or tensile, resulting in different and confusing changes of the mechanical properties.
[33]D. W. Hoffman and M. R. Gaertner, J. Vac. Sci. Technol. **17**, 425 (1980).
[34]A. Niederhofer, P. Nesladek, H. Männling, K. Moto, S. Veprek, and M. Jilek, Surf. Coat. Technol. **120-121**, 173 (1999).
[35]S. Veprek, *Proceedings of the European Materials Research Society*, Strasbourg, France, 1983, edited by P. Pinard and S. Kalbitzer (Les Éditions de Physique, Les Ullis, France, 1984), p. 425.
[36]S. Veprek, F.-A. Sarott, and Z. Igbal, Phys. Rev. B **36**, 3344 (1987).
[37]S. Veprek, O. Nesladek, A. Niederhofer, F. Glatz, M. Jilek, and M. Sima, Surf. Coat. Technol. **108-109**, 138 (1998).
[38]H. Männling, D. S. Patil, K. Moto, M. Jilek, and S. Veprek, Surf. Coat. Technol. **146-147**, 263 (2001).
[39]A. Niederhofer, T. Bolom, P. Nesladek, K. Moto, C. Eggs, D. S. Patil, and S. Veprek, Surf. Coat. Technol. **146-147**, 183 (2001).
[40]H. Schmalzried, *Chemical Kinetics of Solids* (VCH, Weinheim, 1995).
[41]A. R. West, *Solid State Chemistry and its Applications* (Wiley, Chichester, 1984).
[42]G. M. Pharr, Mater. Sci. Eng., A **253**, 151 (1998).
[43]G. M. Pharr and S. V. Hanisworth, Surf. Coat. Technol. **61**, 201 (1993).
[44]H.-H. Behnke, Härterei Zechnische Mitteilungen **48**, 3 (1993).
[45]M. F. Doerner and W. D. Nix, J. Mater. Res. **1**, 601 (1986).
[46]Y. Y. Lim, M. M. Chaudhri, and Y. Enomoto, J. Mater. Res. **14**, 2314 (1999).
[47]S. Veprek, A. Niederhofer, K. Moto, P. Nesladek, H. Männling, and T. Bolom, Mater. Res. Soc. Symp. Proc. **581**, 321 (2000).
[48]A. Niederhofer, Ph.D. thesis, Technical University Munich, 2000.
[49]S. Veprek, A. Niederhofer, K. Moto, T. Bolom, H.-D. Männling, P. Nesladek, G. Dollinger, and A. Bergmaier, Surf. Coat. Technol. **133-134**, 152 (2000).
[50]S. Timoshenko and J. N. Goodier, *Theory of Elasticity*, 2nd ed. (McGraw–Hill, New York, 1951).
[51]The samples of single phase nanocrystalline diamond coatings were kindly provided by Dr. D. Gruen and Dr. A. Krauss from the Argonne National Laboratory. These were the hardest of all diamond coatings which we obtained from various laboratories.
[52]These criteria alone are not sufficient for a correct measurement and interpretation of plastic hardness, because a perfectly elastic soft material, such as rubber, would yield a very high **apparent** plastic hardness. Therefore, one has to consider the whole indentation curve and, in particular, the ''hardness under load'' (''universal hardness'') $H_U = L_{max}/(26.4 \cdot h^2_{max})$, which is equal to the ratio of the maximum applied load and maximum indentation hardness, i.e., it contains the whole elastic and plastic deformation. In such a case, the rubber will show a very high **apparent** plastic hardness but a very low ''hardness under load'' (universal hardness) because of its high elasticity but low stiffness. This fundamental question is related to the meaning of plastic hardness as defined by Mayer and Tabor and the stiffness of materials upon elastic deformation. Because of the limited space available here we refer to the original literature.
[53]E. Mayer Z. Vereins, Deutscher Ingenieure **52**, 645 (1908).
[54]G. Tabor, *The Hardness of Metals* (Clarendon, Oxford, 1951).
[55]D. M. Teter, MRS Bull. **23**, 22 (1998).
[56]M. Hebbache, Solid State Commun. **113**, 427 (2000).
[57]L. A. Davis, Scr. Metall. **9**, 431 (1975).
[58]S. H. Whang, D. E. Polk, and B. C. Giessen, *Proceedings of the 4th International Conference on Rapidly Quenched Metals 1981* (Japan Inst. of Metals, Sendai, 1982), p. 1365.
[59]H. Kimura and T. Masumoto, in *Amorphous Metallic Alloys*, edited by F. E. Luborsky (Butterworths, London, 1983).
[60]X. Jiang, K. Reichelt, and B. Stritzker, J. Appl. Phys. **66**, 5805 (1989).
[61]R. Hill, *The Mathematical Theory of Plasticity* (Oxford University Press, London, 1967).
[62]D. M. Marsh, Proc. R. Soc. London, Ser. A **279**, 420 (1964).
[63]D. M. Marsh, Proc. R. Soc. London, Ser. A **282**, 33 (1964).
[64]Ch. Kittel, *Introduction to Solid State Physics*, 4th ed. (Wiley, New York, 1971).
[65]G. Busch und H. Schade, *Vorlesungen über Festkörperphysik* (Birkhäuser, Basel, 1973).
[66]Cohen *et al.* derived a simple, illustrative formula which describes the bulk moduli of many solids very well: $B = \langle N \rangle / 4(1971 - 220 \cdot \lambda) \cdot x_0^{-3.5}$ Here B is the bulk modulus in GPa, $\langle N \rangle$ is the average coordination number, λ the ''polarity'' of the interatomic bond which decreases the binding energy between two neighbor atoms (the term in parentheses has dimensions GPa $Å^{1.5}$) and x_0 is the equilibrium interatomic distance in

ångströms. It is clear that diamond has the highest bulk modulus because there is no other solid which could simultaneously meet all conditions needed for a maximum value of B, i.e., to form a purely covalent bond ($\lambda=0$) with the shortest interatomic equilibrium distance x_0, the highest binding energy (smallest valence orbitals), and highest coordination number for covalent bond $\langle N\rangle=4$.

[67]M. L. Cohen, Phys. Rev. B **32**, 7988 (1985).

[68]M. L. Cohen, Mater. Sci. Eng., A **209**, 1 (1996).

[69]Strickly speaking, elastic moduli and, in a more general terms, elastic constants are defined at zero pressure. We adhere here to the terminology of ''pressured dependent moduli'' which is frequently used in the literature.

[70]In general case, the stiffness constants $C_{\alpha\beta}$, which are the components of the elastic tensor, are given by the second derivatives of the crystal energy with the constants of the elastic strain tensor $\epsilon_{\alpha\beta}$, i.e., $C_{\alpha\beta}=\delta^2U/\delta{\epsilon_{\alpha\beta}}^2$.

[71]R. Grover, I. C. Getting, and G. C. Kennedy, Phys. Rev. B **7**, 567 (1973).

[72]M. F. Rose, Phys. Status Solidi **17**, K199 (1966).

[73]M. F. Rose, Phys. Status Solidi **21**, 235 (1967).

[74]M. H. Manghnani, Y. Wang, F. Li, P. Zinin, and W. Rafaniello, in *Proceedings of the International Conference on High Pressure Science and Technology*, AIRAPT-17, edited by M. H. Manghnani, W. Nellis, and M. F. Nicol (University Press, India, 2000), p. 945.

[75]J. Evers (private communication).

[76]J. Z. Hu, L. D. Merkle, C. S. Menoni, and I. L. Spain, Phys. Rev. B **34**, 4679 (1986).

[77]Landolt–Börnstein, *Numerical Data and Functional Relationship in Science and Technology*, Group III: Crystal and Solid State Physics, Vol. 1 (Springer, Berlin, 1966), p. 4.

[78]Landolt–Börnstein, in Ref. 77, Vol. 2.

[79]M. H. G. Jacobs and H. A. J. Oonk, Phys. Chem. Chem. Phys. **2**, 2641 (2000).

[80]J. H. Rose, J. R. Smith, F. Guinea, and J. Ferrante, Phys. Rev. B **29**, 2963 (1984).

[81]J. R. Smith, J. Ferrante, P. Vinet, J. G. Gray, R. Richter, and J. Rose, in *Chemistry and Physics of Fracture*, edited by R. M. Latanisos and R. H. Jones (Martinus Nijhoff, Dordrecht, 1987), p. 329.

[82]A. Kelly, W. R. Thyson, and A. H. Cottrell, Philos. Mag. **15**, 567 (1967).

[83]A. S. Argon, in *Glass Science and Technology Vol. 5, Elasticity and Strength of Glasses*, edited by D. R. Uhlmann and N. J. Kreidl (Academic, New York, 1980).

[84]L. N. Sneddon, Int. J. Eng. Sci. **3**, 194 (1965).

[85]A. Bolshakov and G. M. Pharr, Mater. Res. Soc. Symp. Proc. **436**, 189 (1997).

[86]E. H. Yoffe, Philos. Mag. Lett. **77**, 69 (1998).

[87]For other geometry of the indenter this constant changes accordingly but the general dependence remains.

[88]There is always a minimum load which has to be applied to the indenter which causes a minimum pressure under the indenter needed to induce plastic deformation. At a smaller load the material undergoes essentially only elastic deformation.

[89]F. A. McClintock and A. S. Argon, *Mechanical Behavior of Materials* (Addison–Wesley, Reading, MA, 1966), Chap. 13.

[90]This transition appears as a ''noise'' on the loading curve and as a sudden jump of the uloading curve to a lower indentation depth when a maximum load used for the Vickers indenter does not exceed 100 mN. However, if a larger load of $\geqslant$150 mN is used, a similar jump is found upon unloading at about 120–140 mN due to cracking and peeling of the material.

[91]G. M. Pharr, Mater. Res. Soc. Symp. Proc. **239**, 301 (1992).

[92]I. V. Gridneva, Yu. V. Milan, and V. I. Trefilov, Phys. Status Solidi A **14**, 177 (1972).

[93]K. Moto, Ph.D. thesis, Technical University Munich, 2001.

[94]H. Männling, Ph.D. thesis, Technical University Munich (to be published).

[95]W. C. Oliver and G. M. Pharr, J. Mater. Res. **7**, 1564 (1992).

[96]D. Wolf and J. F. Lutsko, Phys. Rev. Lett. **12**, 1170 (1988).

[97]J. A. Jaszczak and D. Wolf, J. Mater. Res. **6**, 1207 (1991).

[98]D. Wolf and J. A. Jaszczak, J. Comput.-Aided Mater. Des. **1**, 111 (1993).

[99]A. A. Voevodin and J. S. Zabinski, Thin Solid Films **370**, 223 (2000).

[100]Hardness of conventional crystalline materials is a measure of the resistance to the motion of a large number of dislocations generated and are able to move through the material in response to shear stress produced by the indenter. Because the line energy of a dislocation is proportional to the shear modulus, the formation and movement of dislocations is more difficult in materials having a high values of G due to a variety of mechanisms involving the resistance to dislocation glide. The shear modulus G can be expressed similarly to Eq. (7) as the second derivative of the total free energy U_{tot} with shear strain

$$c_{ijkl}=V_0^{-1}\frac{\delta^2U_{\text{tot}}}{\delta\gamma_{ij}\delta\gamma_{kl}},$$

where U_{tot} is the total energy of the solid and γ_{ij}, γ_{kl} the tensor strain components. Thus, in addition to a high bond strength also the rigidity of the crystal lattice is important for high hardness. Dislocations and their glide motion play a negligible role in the superhard nanocomposites. The inelastic deformation in such materials is thought to derive entirely from ideal shear processes in the amorphous (liquid-like) component of the nanocomposite with a likely contribution coming from dilatational transformations in both the amorphous and crystalline component in direct analogy to mechanismus operating in glassy solids. These considerations influencing the deformation resistance have also parallels in their fracture resistance where the nanoscale tends to disperse material incompatibilities better before local cavitation can occur.

[101]S. J. Zhou, P. S. Lomdahl, A. F. Voter, and B. L. Holian, Energy Fracture Mech. **61**, 173 (1998).

[102]A. G. Evans, J. Am. Ceram. Soc. **73**, 187 (1990).

[103]B. Derby, Curr. Opin. Solid State Mater. Sci. **3**, 490 (1998).

[104]P. Nesladek, Ph.D. thesis, Technical University Munich, 2000.

[105]P. Holubar, M. Jilek, and M. Sima, Surf. Coat. Technol. **133-134**, 145 (2000).

[106]M. L. Wu, X. W. Lin, V. P. Dravid, Y. W. Chung, M. S. Wong, and W. D. Sproul, J. Vac. Sci. Technol. A **15**, 946 (1997).

[107]D. Li, X. Chu, S. C. Cheng, X. W. Lin, V. P. Dravid, Y. W. Chung, M. S. Wong, and W. D. Sproul, Appl. Phys. Lett. **67**, 203 (1995).

[108]A. A. Voevodin and J. S. Zabinski, J. Mater. Sci. **33**, 319 (1998).

[109]D. Li, X. W. Lin, S. C. Cheng, V. P. Dravid, Y. W. Chung, M. S. Wong, and W. D. Sproul, Appl. Phys. Lett. **68**, 1211 (1996).

[110]Y.-W. Chung, Surf. Rev. Lett. **3**, 1597 (1996).

[111]S. Christiansen, M. Albrecht, H. P. Strunk, and S. Veprek, J. Vac. Sci. Technol. A **14**, 46 (1996).

[112]We would like to emphasize that the suggested nanostructures are based on an extended analysis of the coatings using a variety of techniques which all have a limited accuracy. There is no experimental technique available so far which would allow us to verify the monolayer coverage of the nanocrystals by direct measurement. Therefore, it is improper to speculate about details, such as exactly where the a-$TiSi_2$ is located.

[113]Such a mechanism would lead to a ''pulverization'' of the material within the plastically deformed region which should be observed in high resolution micrographs. This has not been seen for the superhard nanocomposites so far, but more systematic studies are demanding.

[114]The term ''plastic'' deformation implies to certain investigators the crystal plasticity. Since there are many other mechanisms of permanent (irreversible) deformation, e.g., in glasses and amorphous materials, we use here the more general term ''inelastic'' deformation.

[115]The energy of elastic deformation is the area between the unloading curve and the axis of the indentation depth h. Here it is approximately $0.5\times2.7\times10^{-7}$ m$\times7\times10^{-2}$ N$=9.45\times10^{-9}\approx1\times10^{-8}$ J.

[116]The total area of the deformation is about 9×10^{-12} m^2, multiplied with the film thickness of 3.5 μm gives the total deformed volume of about 3×10^{-17} m^3. The elastic energy density is obtained by dividing the elastic energy from the indentation curve of 10^{-8} J by the deformed volume of 3×10^{-17} m^3.

[117]The specific ''molar'' energy of elastic deformation is obtained by multiplying the above estimated energy density by the molar volume which is about 10×10^{-5} m^3 (more exactly 1.15×10^{-5} m^3 for TiN).

[118]Notice that the interatomic bond will break when the dilatation of the interatomic distance reaches 10%–20% of the equilibrium distance x_0 (i.e., the value where the restoring stress reaches the maximum value $[(dE_b/dx)_{\max}$, see Fig. 4(b)] only for a single bond, e.g., in a linear change. In the nanocomposite, however, when the surrounding material is elastically less deformed, the ''cohesion'' of the surrounding material will avoid a complete bond breaking within the flextured region even for a much larger strain.

[119]V. S. Boyko, R. I. Graber, and A. M. Kossevich, *Reversible Crystal Plasticity* (AIP, New York, 1994).

[120]A. S. Argon, Acta Metall. **27**, 47 (1979).

[121]A. S. Argon and L. T. Shi, Acta Metall. **31**, 499 (1983).
[122]A. S. Argon, in *Materials Science and Technology*, edited by R. W. Cahn, P. Haasen, and E. Kramer, Vol. 6: *Plastic Deformation and Fracture of Materials*, edited by H. Mughrabi (VCH, Weinheim, Germany, 1993), pp. 461–508.
[123]S. J. Bull, T. A. Page, and E. H. Yoffe, Philos. Mag. Lett. **59**, 281 (1989).
[124]T. F. Page, W. C. Oliver, and C. J. McHargue, J. Mater. Res. **7**, 450 (1992).
[125]V. V. Bulatov and A. S. Argon, Modell. Simul. Mater. Sci. Eng. **2**, 167 (1994).
[126]C. B. Ponton and R. D. Rawlings, Mater. Sci. Technol. **5**, 865 (1989).
[127]R. Anstis, P. Chantikul, B. R. Lawn, and D. B. Marshall, J. Am. Ceram. Soc. **64**, 533 (1981).
[128]R. A. Cutler and A. V. Virkar, J. Mater. Res. **20**, 3557 (1985).
[129]K. Niihara, J. Ceram. Soc. Jpn. **99**, 974 (1991).
[130]H. Tan and W. Yang, Mech. Mater. **30**, 111 (1998).
[131]Such phenomena are not unique for these nanocomposites alone. Similar effects were also observed in other immiscible alloys in which a nanostructure with an ''optimum'' crystallite size has been formed upon annealing. It has been suggested that such a nanostructure, albeit metastable with respect to large fluctuations, is stable with respect to a change of the specific area of the interface. In the Ni/P alloy, an increase of the hardness after annealing at high temperature has also been found, although the overall range of the achieved hardness was much lower than those in the superhard nanocomposites discussed here.
[132]P. Karvankova, M. G. J. Veprek-Heijman, O. Zindulka, and S. Veprek, Surf. Coat. Technol. (submitted).
[133]J. L. He and S. Veprek, Surf. Coat. Technol. (submitted).
[134]A. S. Argon and S. Veprek, *Proceedings of the 22nd Riso International Symposium on Materials Science: Science of Metastable and Nanocrystalline Alloys, Structure, Properties and Modeling*, edited by A. R. Dinesen *et al.* (Riso Natl. Laboratory, Roskilde, Denmark, 2001), p. 183.
[135]S. Veprek, S. Mukherjee, P. Karvankova, H.-D. Männling, J. L. He, K. Moto, J. Prochazka, and S. Argon, Surf. Coat. Technol. (submitted).